# Observations of Electromagnetic Whistler Precursors at Supercritical Interplanetary Shocks

L.B. Wilson III,[1] A. Koval,[5,1] A. Szabo,[1] A. Breneman,[2] C.A. Cattell,[2] K. Goetz,[2] P.J. Kellogg,[2] K. Kersten,[2] J.C. Kasper[3] B.A. Maruca[3] M. Pulupa[4]

We present observations of electromagnetic precursor waves, identified as whistler mode waves, at supercritical interplanetary shocks using the Wind search coil magnetometer. The precursors propagate obliquely with respect to the local magnetic field, shock normal vector, solar wind velocity, and they are not phase standing structures. All are right-hand polarized with respect to the magnetic field (spacecraft frame), and all but one are right-hand polarized with respect to the shock normal vector in the normal incidence frame. They have rest frame frequencies $f_{ci} < f \ll f_{ce}$ and wave numbers $0.02 \lesssim k\rho_{ce} \lesssim 5.0$. Particle distributions show signatures of specularly reflected gyrating ions, which may be a source of free energy for the observed modes. In one event, we simultaneously observe perpendicular ion heating and parallel electron acceleration, consistent with wave heating/acceleration due to these waves. Although the precursors can have $\delta B/B_o$ as large as 2, fluxgate magnetometer measurements show relatively laminar shock transitions in three of the four events. [Date: 03-27-2012]

## 1. Introduction

Collisionless shock waves, predicted over 50 years ago [*Petschek*, 1958], are a ubiquitous nonlinear structure observed in nearly every space plasma environment. Shock waves require energy dissipation – transfer of energy from one form to another through an irreversible process – where the type of energy dissipation in collisionless shock waves depends upon the Mach number, $M_f$, and has implications for the global structure of the shock wave [*Coroniti*, 1970]. Theory and observations suggest that low Mach number shocks rely upon wave dispersion [*Kennel et al.*, 1985] and/or anomalous resistivity due to wave-particle interactions for energy dissipation [*Sagdeev*, 1966; *Wilson III et al.*, 2007]. Above the first critical Mach number, $M_{cr}$, the shock requires additional energy dissipation in the form of particle reflection to limit wave steepening [*Edmiston and Kennel*, 1984].

Observations of low Mach number quasi-perpendicular (shock normal angle, $\theta_{Bn}$, $\geq 45°$) low-$\beta$ shocks show a relatively laminar transition, with a compressive electromagnetic (EM) precursor wave supplying the dispersive dissipation [*Kennel et al.*, 1985]. The precursor wave has been identified as a right-hand polarized wave with $f_{ci} < f \ll f_{ce}$, where $f_{cs}$ is the cyclotron frequency of species $s$ and i(e) represent ions(electrons), consistent with a whistler mode wave. These 'whistlers' have been observed in nearly every space plasma environment ([*e.g. Wilson III et al.*, 2009, *and references therein*]), can couple to multiple wave modes [*Marsch and Chang*, 1983; *Wu et al.*, 1983; *Matsukiyo and Scholer*, 2006], and can interact with both ions and electrons [*Wu et al.*, 1983]. Recent PIC simulations have found that whistler precursors may play an important role in particle acceleration at higher Mach number shocks [*e.g. Riquelme and Spitkovsky*, 2011]. Thus, whistlers are thought to play an important role in shock wave dynamics through both dispersion and anomalous resistivity.

In this study, we present the first search coil observations of whistler precursors in and around the ramp region of four supercritical interplanetary (IP) shocks observed by the Wind spacecraft. We also present evidence for wave heating and particle acceleration in one event. This work presents the first 3-D magnetic field waveform observations of waves with $f_{sc} \lesssim f_{lh}$ and $f_{lh} < f_{sc} < f_{ce}$ at supercritical IP shocks, where $f_{sc}$ is the spacecraft frame frequency and $f_{lh}$ $(= \sqrt{f_{ce} f_{ci}})$ is the lower hybrid resonance frequency.

## 2. Observations

Waveform captures were obtained from the Wind/WAVES instrument [*Bougeret et al.*, 1995], using the time domain sampler slow (TDSS) receiver, providing three magnetic field components and one electric field component, with 2048 data points sampled at 1875 samples/s. The ambient magnetic field was obtained from the dual, triaxial fluxgate magnetometers [*Lepping et al.*, 1995] sampled at ∼11 samples/s. Ion and electron moments obtained from the Wind/3DP EESA and PESA particle detectors [*Lin et al.*, 1995] were used in conjunction with shock parameters found at [*Kasper*, 2007] to calculate $M_{cr}$, assuming a polytrope index, $\gamma = 5/3$ [*Edmiston and Kennel*, 1984]. Supplemental ion distributions were calculated from the two Faraday Cup (FC) ion instruments from the Wind/SWE experiment [*Ogilvie et al.*, 1995]. For more details about the WAVES and 3DP instruments and analysis, see *Wilson III et al.* [2010].

The top half of Table 1 lists the relevant shock parameters, provided by [*Kasper*, 2007], for the four events presented herein, which include: the shock normal speed in the spacecraft frame, $V_{shn}$; the angle between the shock normal vector and upstream magnetic field, $\theta_{Bn}$; fast mode Mach number, $M_f$; and the shock compression ratio $N_{i2}/N_{i1}$. The bottom half shows the ratios of the $M_f$ to $M_{cr}$ as well as to the three whistler critical Mach numbers [*Krasnoselskikh et al.*, 2002]: $M_w$ corresponds to the maximum Mach number at which a linear whistler can phase stand with respect to the shock; $M_{gr}$ is the maximum Mach number at which the wave can carry energy into the upstream; and $M_{nw}$ is the maximum Mach number for which a stationary solution can be found above which the wave breaks. All four events have $M_f/M_{cr} > 1$ (i.e., are supercritical) and two of the events have $M_f/M_{nw} > 1$.

## 3. Analysis

Figure 1 plots the Wind/MFI data at ∼11 samples/s for the four supercritical IP shocks examined. The only event


0094-8276/12/$5.00

with resolvable magnetic fluctuations is shown in Figure 1**A**. The other three shock profiles show relatively laminar transitions, and magnetic foots are noticeable in Figure 1**B** and 1**D**. All four IP shocks exhibit magnetic overshoots, consistent with previous observations of supercritical shocks [*Farris et al.*, 1993]. Note that Figure 1**A** was examined by *Wilson III et al.* [2009], but only with fluxgate magnetometers. The important observation here is that the magnetic fields are under-sampled and that higher frequency fluctuations (discussed and shown below) with amplitudes comparable to the shock ramp cannot be observed in fluxgate magnetometer data at this sample rate. High time resolution measurements ($\geq$40 samples/s) are needed to resolve the ramp as one can see the spiky nature of these plots is indicative of undersampling.

Figure 2 shows the four TDSS samples that span the ramps of the four supercritical IP shocks. Each panel shows the three normal incidence frame (NIF) components [*defined by Sundkvist et al.*, 2012] of the search coil magnetic field. The ratio of the maximum peak-to-peak wave amplitude to the ambient magnetic field at the start of each event, $\delta B/B_o$, is: (**A**) ∼0.9; (**B**) ∼2.1; (**C**) ∼2.0; and (**D**) ∼0.5. Thus, at least for **B** and **C**, the wave amplitudes significantly modify the ramp structure shown in Figure 1.

The waveforms were analyzed using Minimum Variance Analysis (MVA) [*Khrabrov and Sonnerup*, 1998] to determine the wave vector, **k**; polarization with respect to the ambient magnetic field; and wave normal angles with respect to the local magnetic field ($\theta_{kB}$); shock normal vector ($\theta_{kn}$); and local solar wind velocity ($\theta_{kV}$). Wavelet analysis revealed that these waves exhibit fluctuations at both high ($f_{lh} < f_{sc} < f_{ce}$) and low ($f_{sc} \lesssim f_{lh}$) frequencies. Therefore, we applied multiple standard Fourier bandpass filters to each waveform prior to using MVA on specific subintervals (see *Wilson III et al.* [2009] for more details), requiring that the ratio of the intermediate-to-minimum eigenvalues be >10 to use a result. This analysis resulted in 84 unique **k**-values.

All four precursors are right-hand polarized with respect to the ambient magnetic field, $\mathbf{B}_o$, in the spacecraft frame of reference. Only the precursor shown in Figure 2**B** shows a left-hand polarization in the NIF with respect to the shock normal vector, $\hat{\mathbf{n}}$, the rest are right-handed. The precursors exhibit broad range of values for $\theta_{kB}$, $\theta_{kn}$, and $\theta_{kV}$, consistent with theory [*Wu et al.*, 1983] and prior observations [*Wilson III et al.*, 2009; *Sundkvist et al.*, 2012]. For the low frequency components, the majority had $30^\circ < \theta_{kB} < 75^\circ$, $15^\circ < \theta_{kV} < 45^\circ$, and $15^\circ < \theta_{kn} < 60^\circ$, consistent with previous observations of non-phase standing precursors at IP shocks [*Wilson III et al.*, 2009]. For the high frequency components, the majority had $\theta_{kV}$ and $\theta_{kn} > 45^\circ$, while $\theta_{kB}$ was broad from ∼10° to 90° with most < 60°. Their right-hand polarization with respect to $\mathbf{B}_o$, propagation directions, and frequencies are all consistent with oblique whistler modes in the solar wind.

Since we know $\hat{\mathbf{k}}$ and the solar wind velocity vector is well defined at the start of each TDSS sample, we can use the Doppler-shifted cold plasma dispersion relation for whistlers to estimate the magnitude of the wave vector [*see Coroniti et al.*, 1982]. We found the waves to have $0.03 \lesssim kc/\omega_{pe} \lesssim 4.0$ or $0.02 \lesssim k\rho_{ce} \lesssim 5.0$, where $c$ is the speed of light, $\omega_{pe}$ is the electron plasma frequency, and $\rho_{ce} = V_{Te}/\omega_{pe}$ is the electron thermal gyroradius (where $V_{Te} = \sqrt{2k_BT_e/m_e}$ is the electron thermal speed, $T_e$ the electron temperature, and $k_B$ is Boltzmann's constant). Using these results, we estimated that the precursors had rest frame frequencies $0.01 \lesssim f/f_{lh} \lesssim 10$. These results are consistent with previous solar wind observations [*Coroniti et al.*, 1982] and theory/simulations [*Marsch and Chang*, 1983; *Wu et al.*, 1983; *Lembège et al.*, 2009] of whistlers. At these frequencies, whistlers lie on the same branch of the dispersion relation as both EM lower hybrid [*Marsch and Chang*, 1983] and magnetosonic wave modes [*Wu et al.*, 1983].

We examined the particle distribution functions (Figures 3**i** and 3**e**) from the Wind/3DP instrument for evidence of free energy or signatures of ion reflection. Only three of the events (see Figures 1**A**, 1**B**, and 1**D**) had the burst particle data (full distribution every 3 seconds) needed to examine the distributions in and around the shock ramps. We were able to produce the electron distributions using ∼11 sample/s MFI data, reducing the aliasing across the shock, similar to method introduced by *Schwartz et al.* [2011]. This was not possible for the PESA distributions. However, when we compared the distributions produced using multiple instantaneous magnetic field vectors to those produced using only one (typical method), the results were consistent with each other for the Figure 1**B** event. This is primarily due to the field direction being predominantly in the same direction throughout the duration of the distribution. Thus, we believe that the PESA High distributions produced using only one magnetic field vector (Figure 3**i**) accurately represent the ion distributions across the shock in Figure 1**B**.

All three events with burst particle data showed evidence for gyrating ions (example in Figure 3**i**) at/near the predicted gyrospeed for specular reflection [*Thomsen et al.*, 1983a]. The particle distributions in Figure 3 have color-coded outlines that correspond to the color-coded regions in Figure 1**B**. The IP shock associated with Figure 1**B** also showed evidence for strong perpendicular (with respect to the magnetic field) ion heating (second panel of Figure 3**i**), which was supported by PESA Low and SWE observations. The ion heating is apparent from ∼170-700 km/s (or ∼150-3000 eV proton). This anisotropic heating was not observed in the two other events with burst particle data, yet the magnetic compression ratio is similar for each event ($B_2/B_1$ ≈2.1-2.7, see Figure 1). Therefore, we argue that the observed differences in ion heating are due to the larger waves observed in Figure 2**B**. The observed gyrating ions may provide the free energy for the modes observed in Figure 2, consistent with theory [*Wu et al.*, 1983].

Figure 3**e** shows the three electron distributions, produced using ∼11 sample/s MFI data, at the same times as the ion distributions in Figure 3**i**. The electron distributions show features consistent with previous observations near collisionless shocks [*e.g. Thomsen et al.*, 1983b]. The middle panel shows two interesting features as evidence for parallel electron acceleration. The first, at low energy, is the "bump-on-flattop" feature that is likely due to acceleration of the thermal core by the quasi-static cross shock potential [*Thomsen et al.*, 1983b]. The second, at higher energy, is a shoulder-like feature (shaded magenta region) that has been predicted in multiple simulation studies as the signature of highly oblique waves stochastically accelerating electrons [*e.g. Wu et al.*, 1983; *Cairns and McMillan*, 2005]. The same studies show that these waves also cause perpendicular ion heating of the lower energy ions, consistent with our observations. We also observe higher frequency electrostatic waves near these events, which may explain the flattop distribution in the third panel of Figure 3**e**. However, these waves, which have been examined previously [*Wilson III et al.*, 2007], cannot explain both the perpendicular ion heating and parallel electron acceleration. Therefore, we argue that the wave observed in Figure 2**B** is responsible for the strong anisotropic ion heating in Figure 3**i** and parallel electron acceleration in Figure 3**e**, consistent with the predicted interaction between low frequency (i.e. $\lesssim f_{lh}$) very oblique (i.e. $\theta_{kB} > 75^\circ$) whistler waves and particles [*Wu et al.*, 1983].

Note that the shoulder-like feature in Figure 3**e** is directed toward the downstream. This coupled with the wave in Figure 2**B** having a left-hand polarization in the NIF with respect to $\hat{\mathbf{n}}$ are consistent with a downstream directed phase velocity, consistent with recent instability driven simulation results [*Comişel et al.*, 2011]. The rest of the waves in Figure 2 were consistent with recent observations [*Sundkvist et al.*, 2012] that suggest the precursors are dispersively driven. Though the wave in Figure 2**B** appears to have a downstream directed phase velocity, it may still have an upstream directed group velocity. For instance, the dispersion relation for oblique magnetosonic waves [*e.g. Coroniti*, 1970] gives a range of wave numbers satisfying $0.5 \lesssim (\mathrm{kc})/\omega_{pe} \lesssim 1.0$ where the wave in Figure 2**B** could have upstream directed group velocities but downstream directed phase velocities, which would be consistent with the results of *Sundkvist et al.* [2012]. The downstream directed phase velocity suggests that the wave in Figure 2**B** is receiving some free energy from reflected gyrating ions that are seen in Figure 3**i**.

## 4. Conclusions

We present the first observations of whistler precursor waves at IP shocks above both the first and nonlinear whistler critical Mach numbers. The precursors have large amplitudes ($\delta \mathrm{B}/\mathrm{B}_o \gtrsim 2$), have right-hand polarizations (spacecraft frame) with respect to $\mathbf{B}_o$, and propagate obliquely with respect to $\mathbf{B}_o$ and $\hat{\mathbf{n}}$; thus they are not phase standing. Only one event showed a left-hand polarization with respect to the $\hat{\mathbf{n}}$ in the NIF. The waves have rest frame frequencies $\mathrm{f}_{ci} < \mathrm{f} \ll \mathrm{f}_{ce}$ and wave numbers $0.02 \lesssim \mathrm{k}\rho_{ce} \lesssim 5.0$. Their characteristics are consistent with EM whistlers and EM lower hybrid waves, both modes known to interact with both ions and electrons [*Wu et al.*, 1983].

In one event we simultaneously observe with the wave specularly reflected gyrating ions and electrons showing signatures of parallel acceleration directed downstream. This event was the only precursor that had a left-hand polarization (in NIF) with respect to $\hat{\mathbf{n}}$. These two features are consistent with downstream directed phase velocity, consistent with recent simulation results [*Comişel et al.*, 2011]. Therefore, we argue that the strong perpendicular ion heating and parallel electron acceleration observed was due to interactions of the particles with this mode.

Two of the IP shocks in our study, the 1997-12-10 (**A**) and 1998-09-24 (**C**) events, satisfy $\mathrm{M}_f/\mathrm{M}_w \leq 1$ and $\mathrm{M}_f/\mathrm{M}_{nw} < 1$. Thus, observation of whistler precursors at these two IP shocks is consistent with the theory that phase standing waves limit the dispersion of the shock [*Krasnoselskikh et al.*, 2002] and previous observations [*Farris et al.*, 1993]. However, the 1998-08-26 (**B**) and 2000-02-11 (**D**) events have $\mathrm{M}_f/\mathrm{M}_{nw} > 1$, which means these two IP shocks should not exhibit whistler precursors and should undergo reformation. Non-stationary reformation has been observed at the terrestrial bow shock [*Lobzin et al.*, 2007] and in simulation [*e.g. Comişel et al.*, 2011]. Since the waves observed in our study are not phase standing, it may account for the observations when $\mathrm{M}_f/\mathrm{M}_{nw} > 1$. However, unlike the dispersion driven reformation discussed by *Krasnoselskikh et al.* [2002], the downstream directed phase velocity observed herein suggests mechanisms consistent with instability driven reformation observed by *Comişel et al.* [2011]. We note that the apparent laminar shock transitions observed in Figures 1**B-D** may only be a consequence of undersampling, not a physical transition to a supercritical structure as previous observations suggested [*Farris et al.*, 1993]. We hypothesize that given the right instrumentation, a collisionless shock ramp would be observed to be buried in large amplitude electromagnetic turbulence extending from nearly DC frequencies up through $\mathrm{f}_{ce}$.

We have presented the first waveform observations of waves near and above $\mathrm{f}_{lh}$ simultaneously observed with particle distributions showing the expected signatures of interactions with these wave modes. This study provides further evidence that microinstabilities and turbulence can play a significant role in particle dynamics and energy dissipation at collisionless shocks.

**Acknowledgments.** We thank S.D. Bale, J.R. Wygant, and R. Lysak for useful discussions of the physics involved in our study. All Wind spacecraft data were produced under Wind MO&DA grants. This research was partially supported by NESSF grant NNX07AU72H, grant NNX07AI05G, the Dr. Leonard Burlaga/Arctowski Medal Fellowship, and UCB work sponsored by NASA grant NNX10AT09G.

## References

Bougeret, J.-L., et al. (1995), Waves: The Radio and Plasma Wave Investigation on the Wind Spacecraft, *Space Sci. Rev.*, *71*, 231–263, doi:10.1007/BF00751331.

Cairns, I. H., and B. F. McMillan (2005), Electron acceleration by lower hybrid waves in magnetic reconnection regions, *Phys. Plasmas*, *12*, 102,110–+, doi:10.1063/1.2080567.

Comişel, H., M. Scholer, J. Soucek, and S. Matsukiyo (2011), Non-stationarity of the quasi-perpendicular bow shock: comparison between Cluster observations and simulations, *Ann. Geophys.*, *29*, 263–274, doi:10.5194/angeo-29-263-2011.

Coroniti, F. V. (1970), Dissipation discontinuities in hydromagnetic shock waves, *J. Plasma Phys.*, *4*, 265–+, doi:10.1017/S0022377800004992.

Coroniti, F. V., C. F. Kennel, F. L. Scarf, and E. J. Smith (1982), Whistler mode turbulence in the disturbed solar wind, *J. Geophys. Res.*, *87*, 6029–6044, doi:10.1029/JA087iA08p06029.

Edmiston, J. P., and C. F. Kennel (1984), A parametric survey of the first critical Mach number for a fast MHD shock., *J. Plasma Phys.*, *32*, 429–441.

Farris, M. H., C. T. Russell, and M. F. Thomsen (1993), Magnetic structure of the low beta, quasi-perpendicular shock, *J. Geophys. Res.*, *98*, 15,285–+, doi:10.1029/93JA00958.

Kasper, J. C. (2007), Interplanetary Shock Database, harvard-Smithsonian Center for Astrophysics, Online: *http://www.cfa.harvard.edu/shocks/*.

Kennel, C. F., J. P. Edmiston, and T. Hada (1985), A quarter century of collisionless shock research, in *Collisionless Shocks in the Heliosphere: A Tutorial Review*, *Geophys. Monogr. Ser.*, vol. 34, edited by R. G. Stone and B. T. Tsurutani, pp. 1–36, AGU, Washington, D.C.

Khrabrov, A. V., and B. U. Ö. Sonnerup (1998), Error estimates for minimum variance analysis, *J. Geophys. Res.*, *103*, 6641–6652, doi:10.1029/97JA03731.

Krasnoselskikh, V. V., B. Lembège, P. Savoini, and V. V. Lobzin (2002), Nonstationarity of strong collisionless quasiperpendicular shocks: Theory and full particle numerical simulations, *Phys. Plasmas*, *9*, 1192–1209, doi:10.1063/1.1457465.

Lembège, B., P. Savoini, P. Hellinger, and P. M. Trávn´ıček (2009), Nonstationarity of a two-dimensional perpendicular shock: Competing mechanisms, *J. Geophys. Res.*, *114*, 3217–+, doi:10.1029/2008JA013618.

Lepping, R. P., et al. (1995), The Wind Magnetic Field Investigation, *Space Sci. Rev.*, *71*, 207–229, doi:10.1007/BF00751330.

Lin, R. P., et al. (1995), A Three-Dimensional Plasma and Energetic Particle Investigation for the Wind Spacecraft, *Space Sci. Rev.*, *71*, 125–153, doi:10.1007/BF00751328.

Lobzin, V. V., V. V. Krasnoselskikh, J. Bosqued, J. Pinçon, S. J. Schwartz, and M. Dunlop (2007), Nonstationarity and reformation of high-Mach-number quasiperpendicular shocks: Cluster observations, *Geophys. Res. Lett.*, *34*, 5107–+, doi:10.1029/2006GL029095.

Marsch, E., and T. Chang (1983), Electromagnetic lower hybrid waves in the solar wind, *J. Geophys. Res.*, *88*, 6869–6880, doi: 10.1029/JA088iA09p06869.

Matsukiyo, S., and M. Scholer (2006), On microinstabilities in the foot of high Mach number perpendicular shocks, *J. Geophys. Res.*, *111*, 6104–+, doi:10.1029/2005JA011409.

Ogilvie, K. W., et al. (1995), SWE, A Comprehensive Plasma Instrument for the Wind Spacecraft, *Space Sci. Rev.*, *71*, 55–77, doi:10.1007/BF00751326.

Petschek, H. E. (1958), Aerodynamic Dissipation, *Rev. Mod. Phys.*, *30*, 966–974, doi:10.1103/RevModPhys.30.966.

Riquelme, M. A., and A. Spitkovsky (2011), Electron Injection by Whistler Waves in Non-relativistic Shocks, *Astrophys. J.*, *733*, 63–+, doi:10.1088/0004-637X/733/1/63.

Sagdeev, R. Z. (1966), Cooperative Phenomena and Shock Waves in Collisionless Plasmas, *Rev. Plasma Phys.*, *4*, 23–+.

Schwartz, S. J., E. Henley, J. Mitchell, and V. Krasnoselskikh (2011), Electron Temperature Gradient Scale at Collisionless Shocks, *Phys. Rev. Lett.*, *107*, 215,002, doi: 10.1103/PhysRevLett.107.215002.

Sundkvist, D., V. Krasnoselskikh, S. D. Bale, S. J. Schwartz, J. Soucek, and F. Mozer (2012), Dispersive Nature of High Mach Number Collisionless Plasma Shocks: Poynting Flux of Oblique Whistler Waves, *Phys. Rev. Lett.*, *108*, 025,002, doi: 10.1103/PhysRevLett.108.025002.

Thomsen, M. F., J. T. Gosling, and S. J. Schwartz (1983a), Observational evidence on the origin of ions upstream of the earth's bow shock, *J. Geophys. Res.*, *88*, 7843–7852, doi: 10.1029/JA088iA10p07843.

Thomsen, M. F., S. P. Gary, W. C. Feldman, T. E. Cole, and H. C. Barr (1983b), Stability of electron distributions within the earth's bow shock, *J. Geophys. Res.*, *88*, 3035–3045, doi: 10.1029/JA088iA04p03035.

Wilson III, L. B., C. A. Cattell, P. J. Kellogg, K. Goetz, K. Kersten, L. Hanson, R. MacGregor, and J. C. Kasper (2007), Waves in Interplanetary Shocks: A Wind/WAVES Study, *Phys. Rev. Lett.*, *99*, 041,101–+, doi: 10.1103/PhysRevLett.99.041101.

Wilson III, L. B., C. A. Cattell, P. J. Kellogg, K. Goetz, K. Kersten, J. C. Kasper, A. Szabo, and K. Meziane (2009), Low-frequency whistler waves and shocklets observed at quasi-perpendicular interplanetary shocks, *J. Geophys. Res.*, *114*, 10,106–+, doi:10.1029/2009JA014376.

Wilson III, L. B., C. A. Cattell, P. J. Kellogg, K. Goetz, K. Kersten, J. C. Kasper, A. Szabo, and M. Wilber (2010), Large-amplitude electrostatic waves observed at a supercritical interplanetary shock, *J. Geophys. Res.*, *115*, 12,104–+, doi: 10.1029/2010JA015332.

Wu, C. S., D. Winske, K. Papadopoulos, Y. M. Zhou, S. T. Tsai, and S. C. Guo (1983), A kinetic cross-field streaming instability, *Phys. Fluids*, *26*, 1259–1267, doi:10.1063/1.864285.

L.B. Wilson III, NASA Goddard Space Flight Center, Code 672, Bldg 21, Room 143A, Greenbelt, MD 20771, USA. (lynn.b.wilsoniii@gmail.com)

A. Koval, NASA Goddard Space Flight Center, Greenbelt, MD 20771, Building 21, Room 143A, USA. (andriy.koval-1@nasa.gov)

A. Szabo, NASA Goddard Space Flight Center, Greenbelt, MD 20771, Building 21, Room 156, USA. (adam.szabo-1@nasa.gov)

A. Breneman, School of Physics and Astronomy, University of Minnesota, 116 Church St SE, Minneapolis, MN 55455, USA. (awbrenem@gmail.com)

C.A. Cattell, School of Physics and Astronomy, University of Minnesota, 116 Church St SE, Minneapolis, MN 55455, USA. (cattell@fields.space.umn.edu)

K. Goetz, School of Physics and Astronomy, University of Minnesota, 116 Church St SE, Minneapolis, MN 55455, USA. (goetz@waves.space.umn.edu)

P.J. Kellogg, School of Physics and Astronomy, University of Minnesota, 116 Church St SE, Minneapolis, MN 55455, USA. (pauljkellogg@gmail.com)

K. Kersten, School of Physics and Astronomy, University of Minnesota, 116 Church St SE, Minneapolis, MN 55455, USA. (kkersten@physics.umn.edu)

J.C. Kasper, Harvard-Smithsonian Center for Astrophysics, Perkins 138; MS 58, 60 Garden Street, Cambridge, MA 02138, USA. (jkasper@cfa.harvard.edu)

B.A. Maruca, Harvard-Smithsonian Center for Astrophysics, Perkins 138; MS 58, 60 Garden Street, Cambridge, MA 02138, USA. (bmaruca@cfa.harvard.edu)

M. Pulupa, University of California, Berkeley, Space Sciences Lab, 7 Gauss Way, Berkeley, CA 94720, USA. (pulupa@ssl.berkeley.edu)

**Table 1.** Shock Parameters and Mach Number Ratios

| **Date** | $V_{shn}$ (km/s) | $\theta_{Bn}$ | $M_f$ | $N_{i2}/N_{i1}$ |
|---|---|---|---|---|
| 1997-12-10 | 391 ± 12 | 71° ± 2° | 2.3 ± 0.1 | 2.5 ± 0.4 |
| 1998-08-26 | 687 ± 27 | 82° ± 3° | 4.7 ± 0.2 | 2.9 ± 0.3 |
| 1998-09-24 | 772 ± 96 | 82° ± 2° | 2.9 ± 0.1 | 2.2 ± 0.4 |
| 2000-02-11 | 641 ± 13 | 87° ± 2° | 3.3 ± 0.1 | 3.3 ± 0.5 |
| **Date** | $M_f/M_{cr}$ | $M_f/M_w$ | $M_f/M_{gr}$ | $M_f/M_{nw}$ |
| 1997-12-10 | 1.1 ± 0.2 | 0.3 ± 0.0 | 0.3 ± 0.0 | 0.2 ± 0.0 |
| 1998-08-26 | 2.6 ± 0.4 | 1.6 ± 0.5 | 1.3 ± 0.5 | 1.2 ± 0.4 |
| 1998-09-24 | 1.3 ± 0.2 | 1.0 ± 0.2 | 0.8 ± 0.2 | 0.7 ± 0.2 |
| 2000-02-11 | 1.6 ± 0.2 | 2.5 ± 1.2 | 1.9 ± 1.2 | 1.8 ± 1.1 |

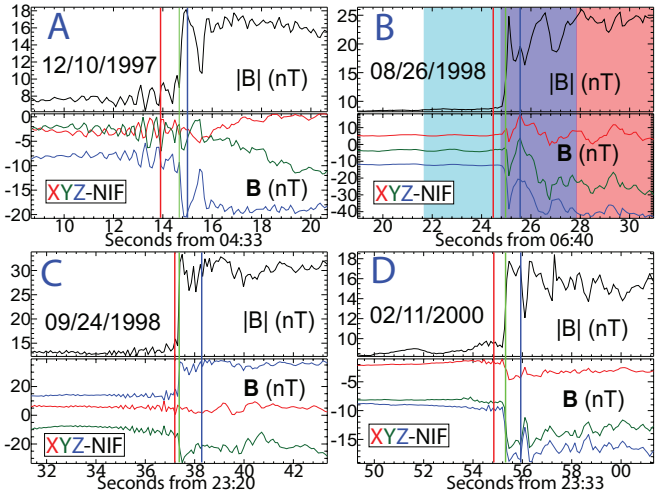


**Figure 1.** Plot of 12-second windows of the Wind fluxgate magnetometer data for the four IP shocks. The top panel for each event plots the magnitude of the magnetic field and the bottom panel plots the three NIF components of the magnetic field defined by *Sundkvist et al.* [2012]. Each event has three vertical lines: the center of the shock ramp (green); and the start (red) and end (blue) times of the associated TDSS sample in Figure 2. The three color-coded shaded regions in panel **B** show the time ranges of the particle distributions shown in Figures 3**i** and 3**e**.

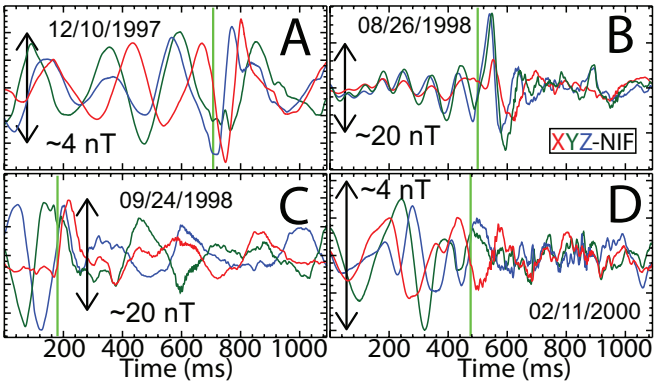


**Figure 2.** Plot of the four unfiltered TDSS samples, identified as magnetosonic-whistler precursor waves, overlapping with the four IP shock ramps. Each panel plots the three NIF components of the magnetic field. The vertical green line in each panel marks the center of the corresponding IP shock ramp in Figure 1. The relative amplitudes of the waveforms are illustrated by the vertical black arrows.

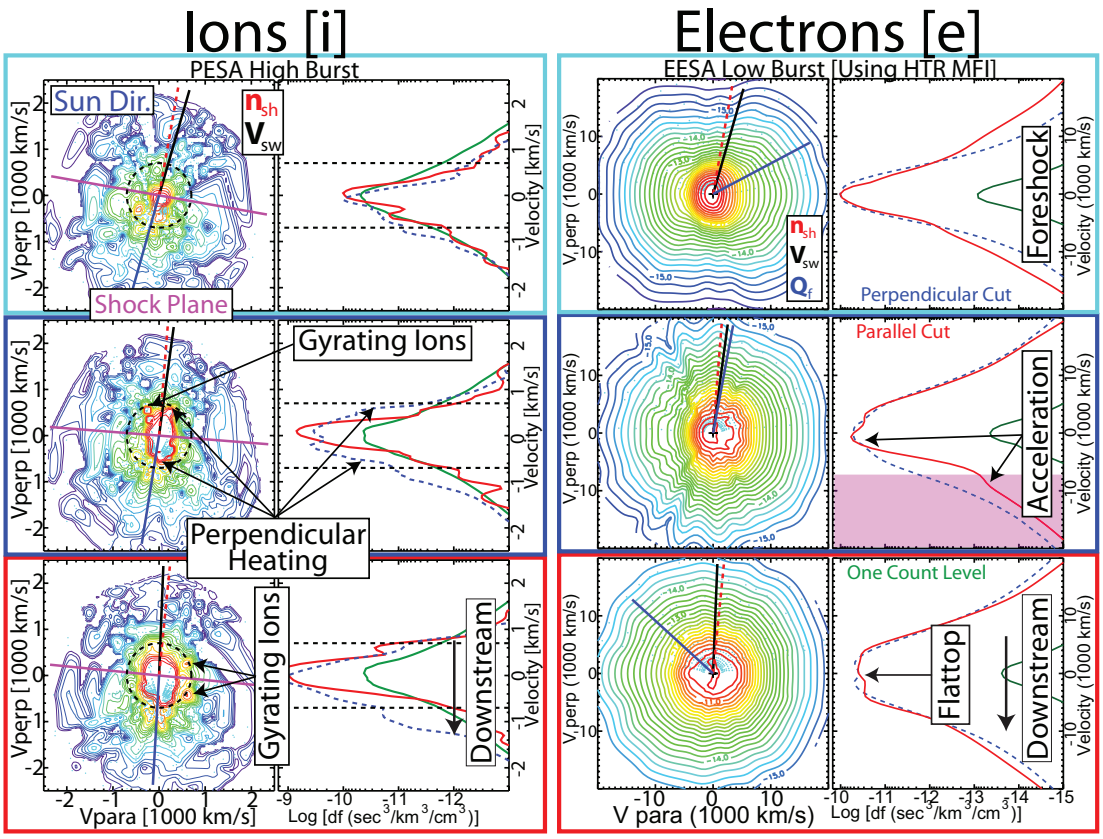


**Figure 3.** The evolution of the particle distributions, ions (**i**) on left and electrons (**e**) on right, across the shock ramp in Figure 1**B**. The contour plots show contours of constant phase space density in the plane containing the ambient magnetic field (horizontal axis of contours) and solar wind velocity. Projected onto this plane are the following: shock normal direction (dashed red line, both **i** and **e**); intersection of the shock plane (solid magenta line, only **e**); solar wind velocity (solid black line, both **i** and **e**); sun direction (solid blue line, only **i**); heat flux vector (solid blue line, only **e**); and a circle (dashed black, only **i**) at ∼700 km/s corresponding to the predicted gyrospeed of specularly reflected ions [*Thomsen et al.*, 1983a]. The right column for each species plots the parallel (solid red line), perpendicular (dashed blue line), and parallel one-count level (solid green line) cuts of the distributions. In the cuts for **i**, horizontal black dotted lines correspond to the circle in the contour plots. In the cuts for **e**, labels defining the respective regions and what we argue to be evidence of parallel electron acceleration are shown.